Biointerface Research in Applied Chemistry
Platinum Open Access Journal (ISSN: 2069-5837)

Article
Volume 12, Issue 1, 2022, 196 - 210
https://doi.org/10.33263/BRIAC121.196210

Associating Graphene Oxide Derivatives to Treat Non-Muscle Invasive Bladder Cancer (NMIBC)

Wagner J. Fávaro [1,*], Joel G. de Souza [1], Mirian Y. Matsumoto [1], Marcela Durán [1], Petra K. Bockelmann [1], Queila C. Dias [1], Nelson Durán [1,2,*]

[1] Laboratory of Urogenital Carcinogenesis and Immunotherapy, Department of Structural and Functional Biology, University of Campinas, Campinas, SP, Brazil; wjfavaro@gmail.com (W.J.F.); joelgsouza82@gmail.com (J.G.S.); manakane@forp.usp.br (M.Y.M.); marceladuranduran@gmail.com (M.D.); petrakarla@hotmail.com (P.K.B.); queilaspg@yahoo.com.br (Q.C.D.); nelsonduran1942@gmail.com (N.D.);
[2] Nanomedicine Research Unit (NanoMed), Federal University of ABC (UFABC), Santo André, SP, Brazil
* Correspondence: wjfavaro@gmail.com (W.J.F.); nelsonduran1942@gmail.com (N.D.);
Scopus Author ID 14037194400 (W.J.F.)
23072832700 (N.D.)
Received: 2.03.2021; Revised: 5.03.2021; Accepted: 8.03.2021; Published: 19.04.2021

Abstract: According to estimates, there were 17,670 bladder cancer-associated deaths in the USA by 2019. Intravesical *Bacillus Calmette-Guerin* (BCG) instillation is used to treat non-muscle invasive bladder cancer (NMIBC). However, more than 40% of BCG administration cases fail to avoid NMIBC relapse and progression. Our aim is to use synthesized GO derivatives to enable the transport of doxorubicin (DOX), a conventional cancer drug, and siRNA to reduce VEGF. Several platforms were tested, and their effects on NMIBC progression were assessed *in vivo* based on histo- and immune analyses. siRNA and GO were covalently bonds to polyethyleneimine (PEI) and polyethylene glycol (PEG) (GO-PEG-PEI/siRNA). DOX bond to oxidized GO was also synthesized. Hybrids were administered *in vivo* (rats) against NMIBC. Histopathology results have shown that hybrids have reduced bladder cancer. The GO-COOH-DOX/GO-PEG-PEI/siRNA potentiated tumor aggressiveness (60%) reduction in animals that did not show signs of lesions. Immunohistochemistry results have shown that the GO hybrid reduced VEGF expression, increased endostatin levels, and low p53 levels were observed. Data analyzed in the current study have shown that hybrid graphene oxides were capable of reducing VEGF expression and have great potential to treat NMIBC.

Keywords: bladder cancer; nanographene oxide; siRNA; doxorubicin.

1. Introduction

According to American Cancer Society, estimates calculated for bladder cancer (BC) (fourth most common cancer) in the United States for 2019, there were 80,470 new cases of the disease: 61,700 among men and 18,770 among women; and 17,670 bladder cancer-associated deaths: 12,870 among men and 4,800 among women [1,2].

Unfortunately, the progress of BC treatment was not effectively designed. Intravesical *Bacillus Calmette-Guerin* (BCG) instillation has been used to treat NMIBC for more than 40 years, and it remains the gold treatment adopted in cases of high- and intermediate-risk disease [3]. Despite the relative success of intravesical BCG administration, more than 40% of applications fail to avoid NMIBC relapse and progression.

BC treatment faces great challenges such as disease relapse and progression even after BCG treatment and treatment availability and patients' tolerability [3]. It is important

highlighting that approximately 40% of patients undergoing BCG treatment can experience progression to the invasive form of BC [3]. Although Mitomycin C (MMC) was used as alternative intravesical therapy, BCG was better than MMC [4-7].

All these factors have encouraged researchers to develop new therapeutic alternatives to treat BC, emphasizing drug delivery systems that enable intravesical drug administration since human bladder tissue is not significantly vascularized, a fact that may limit the effectiveness of treatments based on systemic drug administration. These drug delivery carriers helped enhance therapeutic effectiveness and avoid NMIBC progression to muscle-invasive bladder cancer (MIBC) [8].

Angiogenesis plays a key role in tumor cell growth, development, and invasion during metastatic processes. The vascular endothelial growth factor (VEGF) is one of the important mediators of new vessels' growth expressing vascular endothelial growth factor (VEGFR) [9-11]. Using interfering RNAs, which cleavage the messenger RNA, is one of the methods that have been investigated for this purpose. Thus, scaffolds' use to deliver siRNA targeting VEGF is a relevant strategy to block new vessels' formation and, consequently, inhibit cancer progression [3]. Nano graphene oxide (GO) derivatives have been developed to enable DNA and siRNA delivery [12-15]. The use of GO functionalized with polyethyleneimine (PEI) and with other cationic polymers for DNA and siRNA [15] release has also been investigated to enable GO complexation with siRNA. GO conjugated with PEG (Polyethylene Glycol), and PEI (GO-PEG-PEI) presented significant stability in the presence of salts and serum. The system complexed with siRNA has shown high siRNA transfection efficiency, in addition to reduced cytotoxicity, in comparison to the system complexed with PEI and GO-PEI without PEGylation [16]. Doxorubicin (DOX) and siRNA were associated with GO functionalized with folic acid scaffold used as a platform, a promising model to be used in cancer treatments [15,17].

The current study aimed to use previously synthesized GO derivatives to transport DOX, which is a conventional drug widely used to treat many cancer types, and use siRNA to reduce VEGF. Platforms were tested separately or in combination with one another, and their effects on NMIBC progression were assessed *in vivo* based on histopathological and immunohistochemical analyses.

2. Materials and Methods

2.1. Nano graphene oxide (GO) derivatives.

The characterization of free and functionalized nanoparticles of GO*:* GO, GO-PEG-PEI, GO-COOH, GO-COOH-DOX were previously synthesized and characterized [18].

2.2. In vivo evaluation of graphene oxide derivatives on the NMIBC treatment NMIBC. Induction protocol and treatment.

Seven weeks old Fischer 344 rats were supplied by the Multidisciplinary Center for Biological Investigation (CEMIB) at the University of Campinas (UNICAMP). The ethical principles in animal research (CEUA/IB/ UNICAMP–protocol number: 3795-1) were followed to perform the experiments. Animals were anesthetized for subsequent intravesical catheterization. Five animals (Control group – Group 1) were treated with 0.30 ml of 0.9% NaCl each 14 days during 14 weeks. Moreover, thirty animals received intravesically 1.5

mg/Kg of N-methyl-N-nitrosourea (MNU) dissolved in 0.30 mL of sodium citrate (1M, pH 6.0) for 8 weeks with 14 days of interval between the applications [19,20].

Fourteen days after applying the last dose of MNU, all animals underwent ultrasonography analysis to investigate tumor occurrence. The ultrasonography analysis was performed employing a portable and software-controlled system, equipped with a 10–5 MHz linear array transducer of 38-mm [20]. Control group animals did not show infiltrating mass on the bladder walls (Figure 1A). On the other hand, the MNU group's ultrasonography revealed a mass with an average tumor size of 3.2 X 2.1 mm (Figure 1C).

The animals treated with MNU were divided into 6 groups (n=5): MNU (Group 2), DOX (Group 3), GO-COOH-DOX (Group 4), GO-PEG-PEI (Group 5), GO-PEG-PEI/siRNA (Group 6), and GO-COOH-DOX + GO-PEG-PEI/siRNA (Group 7). For group 2, 0.20 mL of 0.9% saline was administered intravesically once a week for 6 weeks. Groups 3 and 4 were treated with DOX and GO-COOH-DOX, respectively, at doses of 1 mg/Kg intravesically. Groups 5 and 6 underwent the treatment with GO-PEG-PEI and GO-PEG-PEI/siRNA, receiving a dose every 14 days for 6 consecutive weeks (140 µg/Kg, considering the amount of siRNA), intravesically. Finally, group 7 was treated with GO-COOH-DOX once a week for 6 consecutive weeks and GO-PEG-PEI/siRNA each 14 days for the same period, intravesically.

2.3. Histopathological analysis.

Samples (small pieces) of urinary bladders from all animals were surgically extracted and collected and subsequently were analyzed as previously reported [20].

After that, the lesions present in the urinary bladder (UB) were analyzed by a senior uropathologist, according to the Health/World International Society of Urological Pathology Organization [21].

2.4. Immunohistochemistry of VEGF, Endostatin, p53, PI3K, PTEN, BAX, CXCR4, and Nrf2.

To perform the immunolabelings analysis, the same samples used in the histopathological study were employed. The same methodology described before was carried out [20]. In order to investigate the intensity of antigen immunoreactivity, the percentage of positive urothelial cells in the UB was observed in ten fields for each antibody with a magnification of 400x. For performing this analysis, the Image J software (https://imagej.nih.gov/ij/) was used. The intensity of the immunoreactivity was graded on a scale of 0-3. Thus, it was expressed as 0 (immunoreactivity absence), 0% positive urothelial cells; 1 (weak immunoreactivity), 1-35% positive urothelial cells; 2 (moderate immunoreactivity), 36-70% (positive urothelial cells); 3 (intense immunoreactivity), > 70% (positive urothelial cells) [20].

2.5. Statistical analyses.

The proportion test was used to evaluate the histopathological and immune-histochemical results. A type-I error of 5% was statistically significant for all analyses performed.

3. Results and Discussion

3.1. Effect of GO derivatives on NMIBC progression.

3.1.1. Histopathological and ultrasound analyses.

Ultrasound examination was used to investigate tumor incidence in the assessed animals. Figures 1 and 2 present the results of ultrasound and histopathological analyses of the most representative images applied to different experimental groups. There were some correlations between ultrasound images and histopathological analysis.

Based on ultrasound and histopathological analysis results, there were no morphological changes in the UB of animals in the Control group (Figures 1A, 1B). Normal urothelium with the 3 layers formed by umbrella cells was observed (Figure 1B). On the other hand, the UBs of the MNU group presented histopathological changes, malignant neoplastic lesions such as papillary carcinoma - pTa (Figure 1D) in 80% of the animals, and carcinoma *in situ* (pTis) in 20% of them (Table 1). Ultrasound examination has shown a mass (mean tumor size 3.2 X 2.1 mm) infiltrating the ventral, dorsal, and cranial bladder walls (Figure 1C).

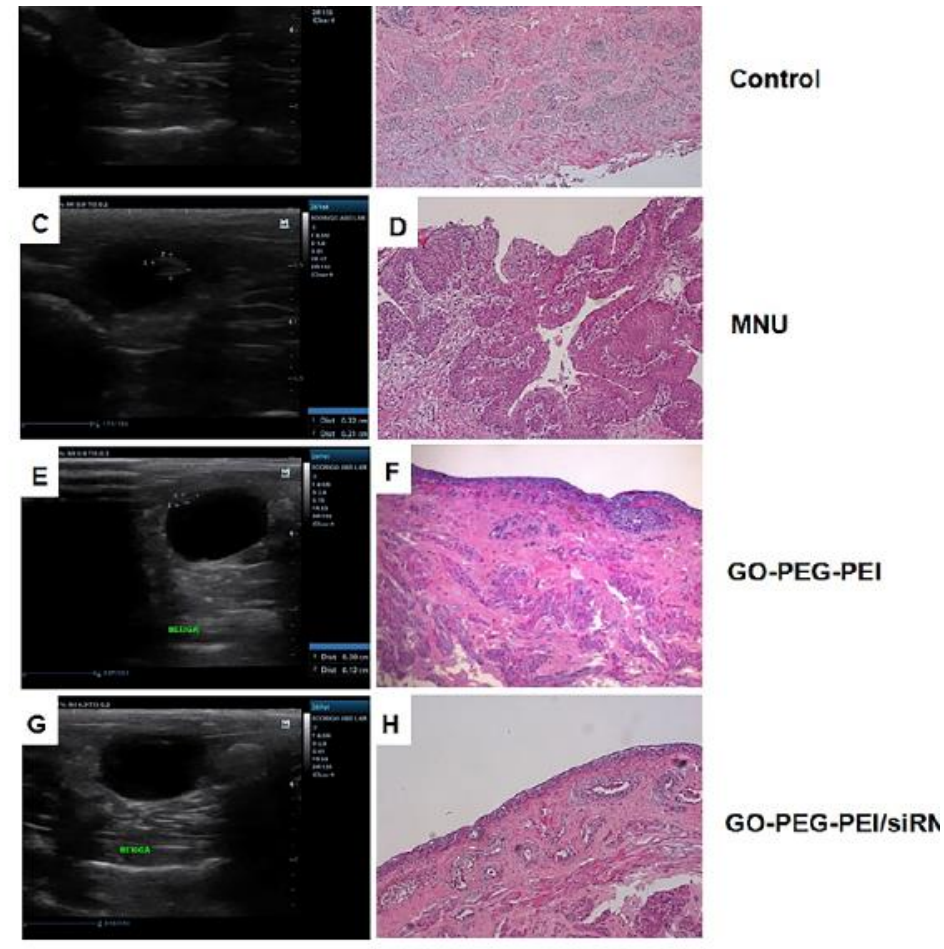

Figure 1. Ultrasonography (A, C, E, and G) and histopathology of the urinary bladder (B, D, F, and H) of the animals from Control, MNU, GO-PEG-PEI, and GO-PEG-PEI/siRNA groups. Control: A (Ultrasonography with no infiltrating mass) and B (normal urinary bladder); MNU: C (Ultrasonography with infiltrating a mass of 3.2 x 2.1 mm) and D (Papillary carcinoma - pTa); GO-PEG-PEI: E (Ultrasonography with infiltrating mass – 3.0 x 1.2 mm) and F (Carcinoma *in situ* - pTis); GO-PEG-PEI/siRNA: G (Ultrasonography with no infiltrating mass) and H (normal urinary bladder). Photomicrographs (B, D, F, and H) at 100X magnification.

Malignant lesions were observed in the UB of all (100%) animals in the group treated with GO-PEG-PEI (Table 1). Based on histopathological analyses, pTis were the most frequent lesions found in this group (Figure 1F), whereas 20% of the animals in it had pTa lesions. Ultrasound examination has revealed infiltrating mass in 100% of the animals (Figure 1E).

Sixty percent (60%) of animals in the group treated with GO-PEG-PEI/siRNA had malignant lesions classified as pTis, 20% of them had pTa, and 20% presented healthy bladder (Figure 1H). Ultrasound examination did not show infiltrating mass in 80% of the assessed animals (Figure 1G). Since NMIBC induction resulted in malignant lesions in 100% of animals (MNU Group), it is possible saying that this treatment enabled tumor progression inhibition (TPI) in 20% of treated animals (Table 1). Thus, the GO-PEG-PEI/siRNA system may have effectively silenced VEGF (restriction to form new vessels and reduced/oxygen supply to the tumor).

According to Table 1, 100% of animals in the DOX group presented lesions classified as pTa, probably to its solubility in water and elimination. Ultrasound examination has revealed infiltrating mass in 100% of the assessed animals (Figures 2A, 2B). DOX (Doxil ®) use to treat NMIBC (3.0 mf/kg) demonstrated that 20% of the animals had benign lesions, whereas 80% of them presented papillary carcinoma malignant lesions *in situ* [22]. It is important mentioning that in the case of carcinoma *in situ*, Valrubicin - which is a DOX analog approved by the Food and Drug Administration (FDA) to treat tumors refractory to BCG immunotherapy - has shown to be ineffective [23].

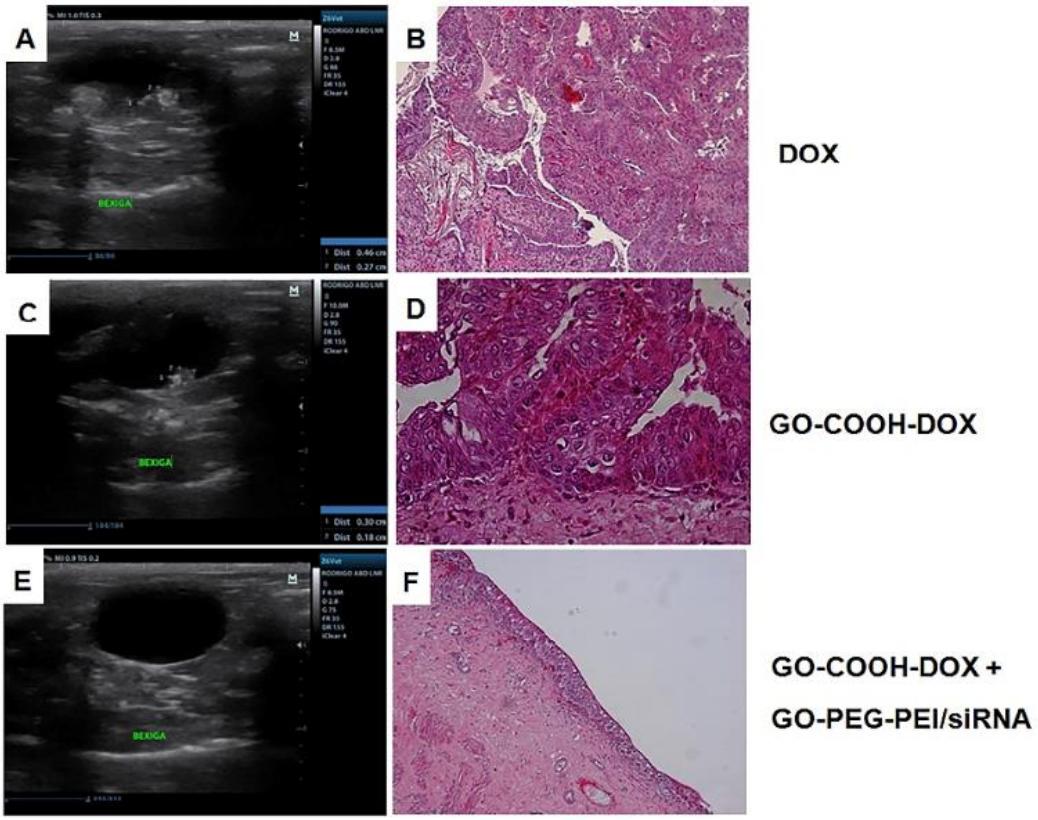

Figure 2. Ultrasonography (A, C, and E) and histopathology of the urinary bladder (B, D, and F) of the animals from DOX, GO-COOH-DOX, and GO-COOH-DOX + GO-PEG-PEI/siRNA groups. DOX: A (Ultrasonography with infiltrating a mass of 4.6 x 2.7 mm) and B (papillary carcinoma - pTa); GO-COOH-DOX: C (Ultrasonography with infiltrating a mass of 3.0 x 1.8 mm) and D (Papillary carcinoma- pTa); GO-COOH-DOX + GO-PEG-PEI/siRNA: E (Ultrasonography with no infiltrating mass) and F (normal urinary bladder). Photomicrographs at 400X (B, F) and 100X (C) magnification.

Ultrasound examination has shown infiltrating mass in 60% of animals in the group treated with GO-COOH-DOX (Figure 2C). Based on histopathological analysis results, 20% of the assessed animals presented pTis, whereas 60% of them had pTa lesions (Figure 2D). However, 20% of the animals presented an uninjured bladder with healthy urothelium. This outcome has shown that tumor progression in this group was successfully inhibited (Table 1).

Table 1. Percentage of histopathological changes of the urinary bladder of rats from different experimental groups.

Experimental Groups (n=5)		Control	MNU	GO-PEG-PEI	GO-PEG-PEI/SiRNA	DOX	GO-COOH-DOX	GO-COOH-DOX + GO-PEG-PEI/SiRNA
Abscence of Lesions	**Normal Urothelium**	100%(5)	-	-	20%(1)	-	20%(1)	60%(3)
	Carcinoma *in situ* (pTis)	-	20%(1)	80%(4)	60%(3)	-	20%(1)	20%(1)
	Papillary carcinoma (pTa)	-	80%(4)	-	20%(1)	100%(5)	60%(3)	20%(1)
	Urothelial carcinoma with invasion of the lamina propria (pT1)	-	-	20%(1)	-	-	-	-
Inhibition of Tumor Progression (ITP)		-	-	-	**20%**	-	**20%**	**60%***

*Represents significant difference compared to MNU group (P <0.05); ITP (Inhibition of Tumor Progression) represents the percentage of non-malignant lesions in each experimental group. In this work, malignants lesions were found and divided as follow: Carcinoma *in situ* (pTis). Papillary carcinoma (pTa) and Urothelial carcinoma with invasion of the lamina propria (pT1).

Tumor progression inhibition (TPI) was statistically higher in the group treated with GO-COOH-DOX+GO-PEG-PEI/siRNA association. In total, 60% of animals in this group presented bladder without lesions and with healthy urothelium (Figure 2F), whereas 20% of them had pTis lesions, and the remaining 20% presented pTa associated with squamous metaplasia (Table 1). Based on the ultrasound analysis, 100% of the assessed animals did not have an infiltrating mass (Figure 2E). It is worth mentioning that these results were more promising than the ones concerning the use of GO-COOH-DOX and GO-PEG-PEI/siRNA separate. This finding suggests that the association between these two systems was effective as NMIBC treatment.

3.1.2. Immunohistochemistry of VEGF, Endostatin, p53, PI3K, PTEN, BAX, CXCR4, and Nrf2.

Table 2 presents the VEGF, Endostatin, p53, PI3K, PTEN, BAX, CXCR4, and Nrf2 immunostaining intensity in the UB of animals in the experimental groups.

According to the current results, VEGF immunoreactivity was more intense in the MNU (Figure 3c), GO-PEG-PEI (Figure 3e), and DOX (Figure 4a) groups than in the other groups (Table 2). Furthermore, VEGF immunoreactivity was moderate in the GO-COOH-DOX group (Figure 4c) and weak in the Control (Figure 3a), GO-PEG-PEI/siRNA (Fig.4g), and GO-PEG-PEI/siRNA + GO-COOH-DOX groups (Figure 4e; Table 2).

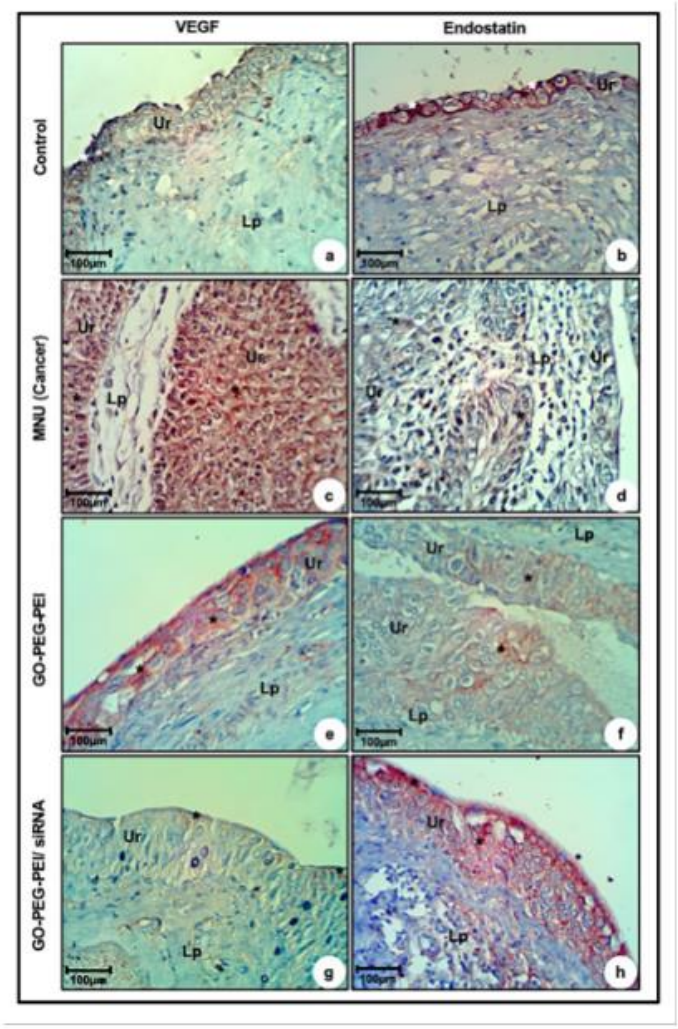

Figure 3. Immunolabelled antigen intensities of the urinary bladder from the Control (a, b), MNU (c, d), GO-PEG-PEI (e, f) and GO-PEG-PEI/ siRNA (g, h) groups. (a), (c), (e), and (g): Immunostaining for VEGF (*) in the urothelium. (b), (d), (f), and (h): Immunostaining for Endostatin (*) in the urothelium. Lp: lamina propria, Ur: urothelium.

Table 2. Semi-quantitative analysis o immunolabelled antigens of the urinary bladder of rats in the different experimental groups.

	Groups						
Antigens	**Control** (n= 5)	**MNU (Cancer)** (n= 5)	**GO-PEG-PEI** (n= 5)	**GO-PEG-PEI/ siRNA** (n= 5)	**DOX**	**GO-COOH-DOX** (n= 5)	**GO-COOH-DOX+ GO-PEG-PEI /siRNA** (n= 5)
VEGF	1 (4.3%) a	3 (97.3%) b	3 (78.4%) b	1 (2.0%) a	3 (78.3%) b	2 (42.6%) c	1 (12.9%) a
Endostatin	3 (93.9%) a	1 (3.7%) b	1 (28.9%) b	2 (65.2%) c	2 (46.5%) c	2 (60.5%) c	3 (90.4%) a
p53	0 (0.0%) a	3 (90.4%) b	3 (86.9%) b	3 (84.1%) b	2 (43.9%) c	2 (38.1%) c	1 (21.2%) c,d
PI3K	1 (2.0%) a	3 (92.4%) b	2 (53.0%) c	1 (11.2%) a	2 (52.4%) c	2 (37.4%) c	1 (10.7%) a
PTEN	3 (95.7%) a	1 (3.0%) b	1 (18.9%) b	2 (61.3%) c	1 (27.4%) b	1 (28.9%) b	3 (85.1%) a
BAX	3 (93.5%) a	1 (2.7%) b	1 (25.9%) c	1 (24.1%) c	2 (66.9%) d	2 (59.2%) d	3 (87.2%) a
CXCR4	1 (21.9%) a	3 (95.0%) b	3 (96.1%) b	3 (95.3%) b	2 (62.0%) c	2 (64.8%) c	1 (26.9%) a
Nrf2	3 (98.4%) a	1 (19.3%) b	1 (11.3%) b	2 (54.1%) c	2 (65.2%) c	2 (68.3) c	3 (97.1%) a

Scores correspond to the intensity of protein immunoreactivity for each group (0 = absent, 1 = weak, 2 = moderate and 3 = strong). Values in parentheses are the median percentage of antigen-positive urothelial cells per group (n = 5 sections/ animal/ group). In the same line, values followed by different letters indicate significant difference between groups ($p < 0.05$).

On the other hand, Endostatin immunoreactivity was significantly higher in the Control (Figure 3b) and GO-COOH-DOX+GO-PEG-PEI/siRNA groups (Figure 4f) than in the other

ones (Table 2). Moreover, moderate immunoreactivity was observed in the GO-COOH-DOX (Figure 4d), GO-PEG-PEI/siRNA (Figure 3h), and DOX groups (Figure 4b). Finally, MNU (Figure 3d) and GO-PEG-PEI groups (Figure 3f) have shown poor immunoreactivity (Table 2). These results corroborated observations made in the histopathological analysis since VEGF and Endostatin levels are directly associated with tumor aggressiveness.

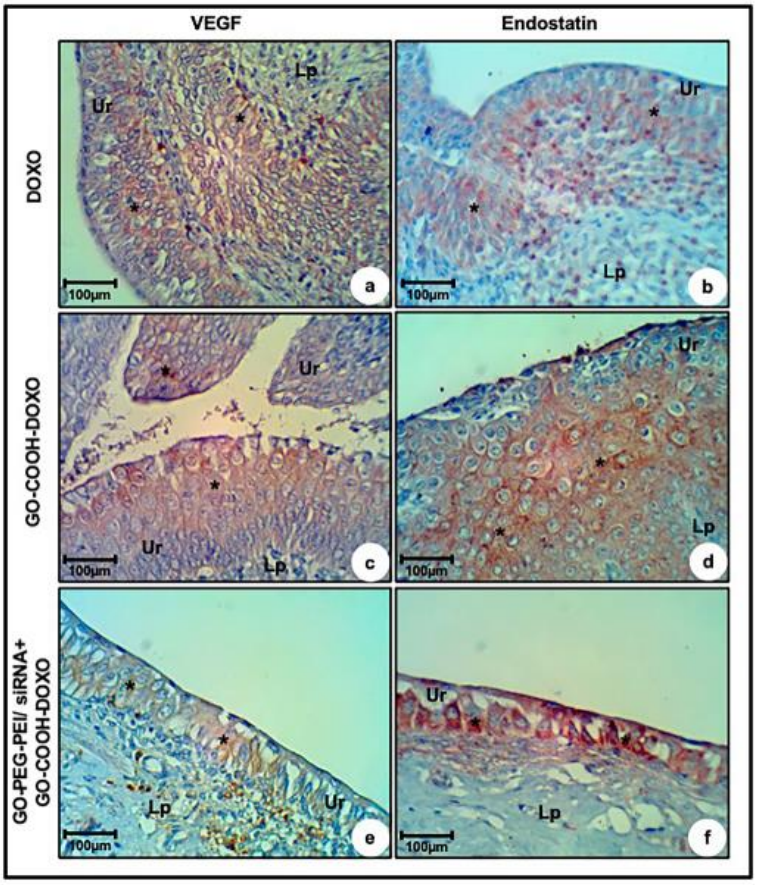

Figure 4. Immunolabelled antigen intensities of the urinary bladder from the DOX (a, b), GO-COOH-DOX (c, d) and GO-COOH-DOX+GO-PEG-PEI/siRNA (e, f) groups. (a), (c) and (e): Immunostaining for VEGF (*) in the urothelium. (b), (d) and (f): Immunostaining for Endostatin (*) in the urothelium. Lp: lamina propria, Ur: urothelium.

The p53 immunostaining has shown possible mutation in this marker in the chemically NMIBC-induced model. Intense immunostaining was observed in the nuclei of urothelial cells in the MNU (Figure S1d; Table 2), GO-PEG-PEI (Figure S1g; Table 2), and GO-PEG-PEI/siRNA groups (Figure S1j; Table 2). Also, p53 immunoreactivities were moderate in the DOX (Figure S2a; Table 2) and GO-COOH-DOX (Figure S2d; Table 2) groups and weak in the GO-COOH-DOX/GO-PEG-PEI/siRNA (Figure S2g; Table 2). Finally, there was no p53 immunostaining in the urothelial cell nuclei of animals in the Control group (Figure S1a; Table 2).

PI3K analysis has shown intense immunoreactivity in animals in the MNU group (Figure S1e) in comparison to other experimental groups (Table 2). Moderate immunoreactivity was observed in the GO-PEG-PEI (Figure S1h), DOX (Figure S2b), and GO-COOH-DOX (Figure S2e) groups, whereas the GO-PEG-PEI/siRNA (Figure S1k) and GO-COOH-DOX+GO-PEG-PEI/siRNA groups (Figure S2h) expressed weak immunoreactivity (Table 2).

However, PTEN immunostaining was much more intense in animals from Control (Figure S1c) and GO-COOH-DOX+GO-PEG-PEI/siRNA (Figure S2i) groups than in the ones in the other experimental groups (Table 2). Animals in the MNU (Figure S1f), GO-PEG-PEI (Figure S1i), DOX (Figure S2c), and GO-COOH-DOX (Figure S2f) groups have shown weak immunoreactivity. Finally, animals in the GO-PEG-PEI/siRNA (Fig. S1l) group presented moderate immunoreactivity (Table 2).

BAX immunostaining was more reactive in animals in the Control (Figure S3a) and GO-COOH-DOX+GO-PEG-PEI/siRNA (Figure S4g) groups than in the ones in the other experimental groups (Table 2). Animals in the DOX (Figure S4a) and GO-COOH-DOX (Figure S4d) groups have shown moderate immunoreactivity, whereas the ones in the MNU (Figure S3d), GO-PEG-PEI (Figure S3g), and GO-PEG-PEI/siRNA (Figure S3j) groups presented weak immunoreactivity (Table 2).

However, animals in the MNU (Figure S3e), GO-PEG-PEI (Figure S3h), and GO-PEG-PEI/siRNA (Figure S3k) groups presented intense CXCR4 immunostaining in comparison to animals in the other groups (Table 2). Immunostaining of animals in the DOX (Figure S4b) and GO-COOH-DOX (Figure S4e) groups was moderate, whereas animals in the GO-COOH-DOX+GO-PEG-PEI/siRNA (Figure S4h) group presented weak immunoreactivity (Table 2).

Finally, Nrf2 immunostaining was intense in animals in the Control (Figure S3c) and GO-COOH-DOX+GO-PEG-PEI/siRNA (Figure S4i) groups in comparison to animals in the other groups (Table 2). Moderate immunostaining was observed in animals from GO-PEG-PEI/siRNA (Figure S3l), DOX (Figure S4c) and GO-COOH-DOX (Figure S4f) groups, whereas animals in the MNU (Figure S3f) and GO-PEG-PEI (Figure S3i) groups presented weak immunoreactivity (Table 2).

According to studies available in the literature, the main function of the MDM2 protein lies in interacting with tumor suppressor p53 to inhibit apoptosis [24-26]. On the other hand, there are circumstances when the inhibitory properties of MDM2 over p53 expression are blocked by PTEN, such as when PTEN sequesters MDM2 in the cytoplasm [27]. PTEN is a tumor suppressor gene [28,29] that acts in apoptosis regulation and cancer suppression [30,31].

PTEN has inhibitory activity in the PI3k/Akt pathway. Akt is activated when PTEN is underexpressed [32]. On the other hand, activated Akt has an anti-apoptotic function in different pathways, including in MDM2 phosphorylation, inhibiting apoptosis [33]. Briefly, PI3k/Akt signaling activation enables MDM2 phosphorylation and inhibits p53. On the other hand, MDM2 phosphorylation by PI3k/Akt signaling decreases when PTEN blocks PI3k/Akt, leading to increased p53 levels and apoptosis induction. According to Table 2, PTEN was up-regulated in the GO-COOH-DOX + GO-PEG-PEG/siRNA group, whereas the expression of these proteins in the GO-COOH-DOX and GO-PEG-PEG/siRNA groups was weak and moderate, respectively. Based on these results, the association between drug delivery platforms was very important to enable an almost complete PTEN expression.

The wild-type p53 was able to suppress and control cell proliferation and kill abnormal cells [34]. On the other hand, p53 mutations can allow cell proliferation [35,36] and are often observed in many cancer types [37]. It is important to point out that endostatin can inhibit tumor growth without affecting cell proliferation [38,39]; p53 is a suppressor protein that inhibits angiogenesis, and consequently, it indirectly inhibits apoptosis. Studies have shown that the wild-type p53 can provide a non-angiogenic phenotype to tumors [40]. The non-angiogenic phenotype results from two angiogenesis inhibitors, namely: endostatin and tumstatin [41]. These proteins derive from collagens 18 and 4, respectively. This process is associated with

the up-regulation of the α(II) collagen prolyl-4-hydroxylase enzyme by the wild-type p53 phenotype [40]. On the other hand, p53 mutation or inactivation leads to a higher cell proliferation rate than apoptosis; consequently, the tumor phenotype becomes angiogenic [33]. According to results in the current study, the GO-COOH-DOX + GO-PEG-PEG/siRNA group has shown low p53 and high Endostatin levels. It is possible assuming that the low p53 levels were associated with the wild-type of this protein and that the high Endostatin levels have provided a non-angiogenic phenotype to the analyzed tumors. Such an assumption could explain the promising results recorded for the group mentioned above.

Bax protein is a Bcl-2 protein homolog that accounts for apoptosis induction. Protein CXCR4 is associated with tumor invasion and metastases that reach high levels in tumors [42]. Suppose one takes into consideration the antiangiogenic properties of the GO-PEG-PEG/siRNA + GO-COOH-DOX association. In that case, it is possible assuming that the drug delivery platforms adopted in the current study decreased the formation of new blood vessels and, subsequently, induced necrosis and cell death. Simultaneously, it was possible observing increased Endostatin levels and tumor volume reduction. PTEN was activated, and tissue repair took place; consequently, BAX was up-regulated in the new normal cell population. CXCR4 also decreased under these conditions, as evidenced by comparing MNU and GO-PEG-PEG/siRNA + GO-COOH-DOX groups. PTEN and BAX were down-regulated in animals in the MNU group, whereas CXCR4 was up-regulated in animals. On the other hand, opposite events were observed for GO-COOH-DOX+GO-PEG-PEG/siRNA association. CXCR4 levels likely decreased due to tumor cell reduction.

4. Conclusions

Based on findings in the current study, GO derivatives were effective in treating NMIBC. The GO-PEG-PEI system showed high dispersibility in an aqueous medium; it also showed high stability and allowed resuspension for applications *in vivo*. The GO-PEG-PEI nanostructure enabled siRNA complexation, even at low concentrations. The GO-COOH-DOX combination was more effective in decreasing NMIBC progression than the DOX-free treatment. On the other hand, the GO-PEG-PEI/siRNA system was more effective in decrease NMIBC progression than DOX-free and GO-COOH-DOX. The GO-COOH-DOX + GO-PEG-PEI/siRNA association was certainly the most promising strategy adopted in the current study since it enabled tumor progression inhibition in 60% of the assessed animals - such data are relevant to the urology field. Ultrasound used to assess NMIBC progression was another highlight in the current study. Despite some limitations, ultrasound results have corroborated the histopathological analyses to some extent. Based on the immunohistochemical analyses, GO-PEG-PEI/siRNA was more effective in reducing VEGF expression than the other groups. The GO-PEG-PEI/siRNA + GO-COOH-DOX association led to higher Endostatin levels than the administration of these systems separate. The high p53 levels observed in animals in the MNU group can be associated with the mutated form of this protein, whereas low levels of it in animals in the GO-COOH-DOX + GO-PEG-PEI/siRNA group may be associated with the wild-type p53. Therefore, if one considers these results altogether, it is possible saying that graphene oxide hybrids have great potential to be used to treat NMIBC.

Funding

This research was funded by São Paulo Research Foundation (FAPESP grant 2014/11154-1), the Brazilian National Council for Scientific and Technological Development (CNPq grant 552120/2011-1).t

Acknowledgments

The authors would like to thank the São Paulo Research Foundation (FAPESP grant 2014/11154-1), the Brazilian National Council for Scientific and Technological Development (CNPq grant 552120/2011-1) for financial support.

Conflicts of Interest

The authors declare no conflict of interest.

Ethical Approval

All procedures performed in studies involving animals were in accordance with the institutional and/or national research committee's ethical standards and its later amendments or comparable ethical standards.

Informed Consent

All persons gave their informed consent to use their data for this retrospective study.

References

1. American Cancer Society. Key Statistics for Bladder Cancer 2019. Available online: https://www.cancer.org/cancer/bladder-cancer/about/key-statistics.html.
2. Malats, N.; Real, F.X. Epidemiology of bladder cancer. *Hematol/Oncol Clinics* **2015**, *29*, 177-189, https://doi.org/10.1016/j.hoc.2014.10.001.
3. Douglass, L.; Schoenberg, M. The future of intravesical drug delivery for non-muscle invasive bladder cancer. *Bladder Cancer* **2016,** *2*, 285-292, https://doi.org/10.3233/BLC-160056.
4. Bohle, A.; Jocham, D. Bock, P.R. Intravesical bacillus *Calmette-Guerin* versus mitomycin C for superficial bladder cancer: A formal meta-analysis of comparative studies on recurrence and toxicity. *J Urol* **2003**, *169*, 90-95, https://doi.org/10.1097/01.ju.0000039680.90768.b3.
5. Wołacewicz, M.; Hrynkiewicz, R.; Grywalska, E.; Suchojad, T.; Leksowski, T.; Rolinski, J.; Niedzwiedzka-Rystwej, P. Immunotherapy in bladder cancer: Current Methods and Future Perspectives. *Cancers* **2020**, *12*, 1181; https://doi.org/10.3390/cancers12051181.
6. Wroclawski, M.L.; Schutz, F.A.; Cha, J.D.; Soares, A. Alternative therapies to Bacillus Calmette-Guerin shortage for nonmuscle'Invasive bladder cancer in Brazil and 0ther underdeveloped countries: Management considerations. *J Global Oncol* **2019**, *2009*, 1-9, https://doi.org/10.1200/JGO.19.00112.
7. Schmidt, S.; Kunath, F.; Coles, B.; Draeger, D.L.; Krabbe, L.M. Dersch, R.; Kilian, S.; Jensen, K.; Dahm, P.; Meerpohl, J.J. Intravesical Bacillus Calmette-Guérin versus mitomycin C for Ta and T1 bladder cancer. *Cochrane Database Syst Rev* **2020**, https://doi.org/10.1002/14651858.CD011935.pub2.
8. Martin, D.T.; Hoimes, C.J.; Kaimakliotis, H.Z.; Cheng, C.J.; Zhang, K.; Liu, L.; Wheeler, M.A.; Kelly, W.K.; Tew, G.N., W. Saltzman, W.M.; Robert M. Weiss, R.M. Nanoparticles for urothelium penetration and delivery of the histone deacetylase inhibitor belinostat for treatment of bladder cancer. *Nanomedicine: Nanotechnology, Biology and Medicine* **2013**, *9*, 1124-1134, https://doi.org/10.1016/j.nano.2013.05.017.
9. Alkhazraji, A.; Elgamal, M.; Ang, S.H.; Shivarov, V. All cancer hallmarks lead to diversity. *Int J Clin Exp Med* **2019**, *12*, 132-157.
10. Chen, Y.; Huang, L. Tumor-targeted delivery of siRNA by non-viral vector: safe and effective cancer therapy. *Expert Opin Drug Deliv* **2008**, *5*, 1301-1311, https://doi.org/10.1517/17425240802568505.

11. Subhan, M.A.; Torchilin, V.P. Efficient Nanocarriers of siRNA Therapeutics for Cancer Treatment. *Transl Res* **2019**. *214*, P62-91, https://doi.org/10.1016/j.trsl.2019.07.006.
12. Pei, X.; Zhu, Z.; Gan, Z.; Chen, J.; Zhang, X., Cheng, X.; Wan, Q.; Wang, KJ. PEGylated nanographene oxide as a nanocarrier for delivering mixed anticancer drugs to improve anticancer activity. Sci Rep **2020**, *10*, https://doi.org/10.1038/s41598-020-59624-w.
13. Zhou, T.; Zhou, X.; Xing, D. Controlled release of doxorubicin from graphene oxide based charge-reversal nanocarrier. *Biomaterials* **2014**, *35*, 4185-4194, https://doi.org/10.1016/j.biomaterials.2014.01.044.
14. Zhang, J.; Feng, L.; Tan, K.; Shi, X.; Xu, L.; Liu, Z.; Peng, R. Dual-polymer-functionalized nanoscale graphene oxide as a highly effective gene transfection agent for insect cells with cell-type-dependent cellular uptake mechanisms. *Part Part Syst Charact* **2013**, *30*, 794-803, https://doi.org/10.1002/ppsc.201300107.
15. Huang, Y.P.; Hung, C.M.; Hsu, Y.C.; Zhong, C-Y.; Wang, W-R.; Chang, C-C.; Lee, M-J. Suppression of breast cancer cell migration by small interfering RNA delivered by polyethylenimine-functionalized graphene oxide. *Nanoscale Res Lett* **2016**, *11*, 247, https://doi.org/10.1186/s11671-016-1463-0.
16. Jain, V.P.; Chaudhary, S.; Sharma, D.; Dabas, N.; Lalji, R.S.K.; Singh, B.K.; Jaiswar, G. Advanced functionalized nanographene oxide as a biomedical agent for drug delivery and anti-cancerous therapy: A review. *Eur Polym J* **2021,** *142*, 110124, https://doi.org/10.1016/j.eurpolymj.2020.110124.
17. Lu, T.; Nong, Z.; Wei, L.; Wei, M.; Li, G.; Wu, N.; Liu, C.; Tang, B.; Qin, Q.; Li, X.; Meng, F. Preparation and anti-cancer activity of transferrin/folic acid double-targeted graphene oxide drug delivery system. *J Biomat Appl* **2020,** *35*, 15–27, https://doi.org/10.1177/0885328220913976.
18. Fávaro, W.J.; De Souza, J.G.; Ferreira, L.A.B.; de Jesus, M.B.; Durán, M.; Bockelmann, P.K.; Bernardes, J.S.; Durán, N. Hybrid graphene oxide as carrier of doxorubicin: cytotoxicity and preliminary *in vivo* assays against bladder cancer. *Adv Nat Sci: Nanosci Nanotechnol* **2020**, *11*, 025016, https://doi.org/10.1088/2043-6254/ab9194.
19. Fávaro, W.J.; Nunes, O.S.; Seiva, R.R.F.; Nunes, I.S.; Woolhiser, L.K.; Durán, N.; Lenaerts, A.J. Effects of P-MAPA immunomodulator on toll-like receptors and p53: Potential therapeutic strategies for infectious diseases and cancer. *Infect Agent Cancer* **2012**, *7*, https://doi.org/10.1186/1750-9378-7-14.
20. Garcia, P.V.; Seiva, F.R., Carniato, A.P.; de Mello Júnior, W.; Durán, N.; Macedo, A.M.; de Oliveira, A.G.; Romih, R.; Nunes, I.S.; Nunes, O.S.; Fávaro, W.J. Increased toll-like receptors and p53 levels regulate apoptosis and angiogenesis in non-muscle invasive bladder cancer: mechanism of action of P-MAPA biological response modifier. *BMC Cancer* **2016**, *16*, https://doi.org/10.1186/s12885-016-2474-z.
21. Epstein, J.L.; Amin, M.B.; Reuter, V.R.; Mostofi, F.K. The World Health Organization/International Society of Urological Pathology consensus classification of urothelial (transitional cell) neoplasms of the urinary bladder. Bladder Consensus Conference Committee. *Am J Surg Pathol* **1998**, *22*, 1435-1448, https://doi.org/10.1097/00000478-199812000-00001.
22. Dias, Q.C.; Nunes, I.S.; Garcia, P.V.; Fávaro, W.J. Potential therapeutic strategies for non-muscle invasive bladder cancer based on association of intravesical immunotherapy with p-MAPA and systemic administration of cisplatin and doxorubicin. *Int Braz J Urol* **2016**, *42*, 942-954, https://doi.org/10.1590/S1677-5538.IBJU.2015.0381.
23. Chehroudi, A.C.; Black, P.C. Emerging intravesical therapies for the management of bacillus *Calmette-Guérin* (BCG)-unresponsive non-muscle-invasive bladder cancer: Charting a path forward, *Can Urol Assoc J* **2020**, *14*, 204-213, http://dx.doi.org/10.5489/cuaj.6101.
24. Wu, C-E.; Pan, Y-R.; Yeh, C-N.; Lunec, J. Targeting P53 as a future strategy to overcome gemcitabine resistance in biliary tract cancers. *Biomolecules* **2020**, *10*, 1474, https://doi.org/10.3390/biom10111474.
25. Li, W.; Peng, X.; Lang, J.; Xu, C. Targeting mouse double minute 2: Current concepts in DNA damage repair and therapeutic approaches in cancer. *Front Pharmacol* **2020,** *11*, 631, https://doi.org/10.3389/fphar.2020.00631.
26. Mayo, L.D.; Dixon, J.E.; Durden, D.; Tonks, N.K.; Donner, D.B. PTEN protects p53 from mdm2 and sensitizes cancer cells to chemotherapy. *J Biol Chem* **2002**, *277*, 5484-5489, https://doi.org/10.1074/jbc.m108302200.
27. Vidotto, T.; Melo, C.M.; Castelli, E.; Koti, M., dos Reis, R.B.; Squire, J.A. Emerging role of PTEN loss in evasion of the immune response to tumours. *Br J Cancer* **2020,** *122*, 1732–1743, https://doi.org/10.1038/s41416-020-0834-6.
28. Parson, R. Discovery of the PTEN tumor suppressor and its connection to the PI3K and AKT oncogenes. *Cold Spring Harb Perspect Med* **2020**, *10*, a036129, https://doi.org/10.1101/cshperspect.a036129.

29. Di Cristofano, A.; Pandolfi, P.P. The multiple roles of PTEN in tumor suppression. *Cell* **2000**, *100*, 387-390, https://doi.org/10.1016/S0092-8674(00)80674-1.
30. Huang, H.; Cheville, J,C,; Pan, Y. Roche, P.C.; Schmidt, L.J.; Tindall, D.J. PTEN induces chemosensitivity in PTEN-mutated prostate cancer cells by suppression of Bcl-2 expression. *J Biol Chem* **2001**, *276*, 38830-38836, https://doi.org/10.1074/jbc.M103632200.
31. Turnham, D.J.; Bullock, N., Dass, M.S.; Staffurth, J.N.; Pearson, H.B. The PTEN Conundrum: How to PTEN-deficient prostate cancer. *Cells* **2020**, *9*, 2342, https://doi.org/10.3390/cells9112342.
32. Ashcroft, M.; Ludwig, R, Woods, D.B.; Copeland, T.D.; Weber, H.O.; MacRae, E.J.; Vousden, K.H. Phosphorylation of HDM2 by Akt. *Oncogene* **2002**, *21*, 1955-1962, https://doi.org/10.1038/sj.onc.1205276.
33. Folkman; J. Tumor suppression by p53 is mediated in part by the antiangiogenic activity of endostatin and tumstatin. *Sci STKE* **2006**, *2006*, pe35, https://doi.org/10.1126/stke.3542006pe35.
34. Ghatak, D.; Das Ghosh, D.; Roychoudhury, S. Cancer Stemness: p53 at the Wheel. *Front Oncol* **2021**, *10*, 604124, https://doi.org/10.3389/fonc.2020.604124.
35. Feroz, W.; Sheikh, A.M.A. Exploring the multiple roles of guardian of the genome: P53. *Egypt J Med Hum Genet* **2020**, *21*, 49, https://doi.org/10.1186/s43042-020-00089-x.
36. Royds, J.A.; Lacopetta, B. p53 and disease: when the guardian angel fails. *Cell Death Differ* **2006**, *13*, 1017-1026, https://doi.org/10.1038/sj.cdd.4401913.
37. Folkman, J. Antiangiogenesis in cancer therapy--endostatin and its mechanisms of action. *Exp Cell Res* **2006**, *312*, 594-607, https://doi.org/10.1016/j.yexcr.2005.11.015.
38. Carmeliet, P. Angiogenesis in life, disease and medicine. *Nature* **2005**, *438*, 932-936, https://doi.org/10.1038/nature04478.
39. Holmgren, L.; Jackson, G.; Arbiser, J. p53 induces angiogenesis-restricted dormancy in a mouse fibrosarcoma. *Oncogene* **1998**, *17*, 819-824, https://doi.org/10.1038/sj.onc.1201993.
40. Teodoro, J.G.; Parker, A.E.; Zhu, X.; Green, M.R. p53-Mediated inhibition of angiogenesis through up-regulation of a collagen prolyl hydroxylase. *Science* **2006**, *313*, 968-971, https://doi.org/10.1126/science.1126391.
41. Warren, C.F.A.; Wong-Brown, M.W.; Bowden, N.A. BCL-2 family isoforms in apoptosis and cancer. *Cell Death Dis* **2019**, *10*, https://doi.org/10.1038/s41419-019-1407-6.
42. Poeta, V.M.; Massara, M.; Capucetti, A.; Bonecchi, R. Chemokines and chemokine receptors: New targets for cancer immunotherapy. *Front Immunol* **2019**, *10*, https://doi.org/10.3389/fimmu.2019.00379.

Supplementary materials

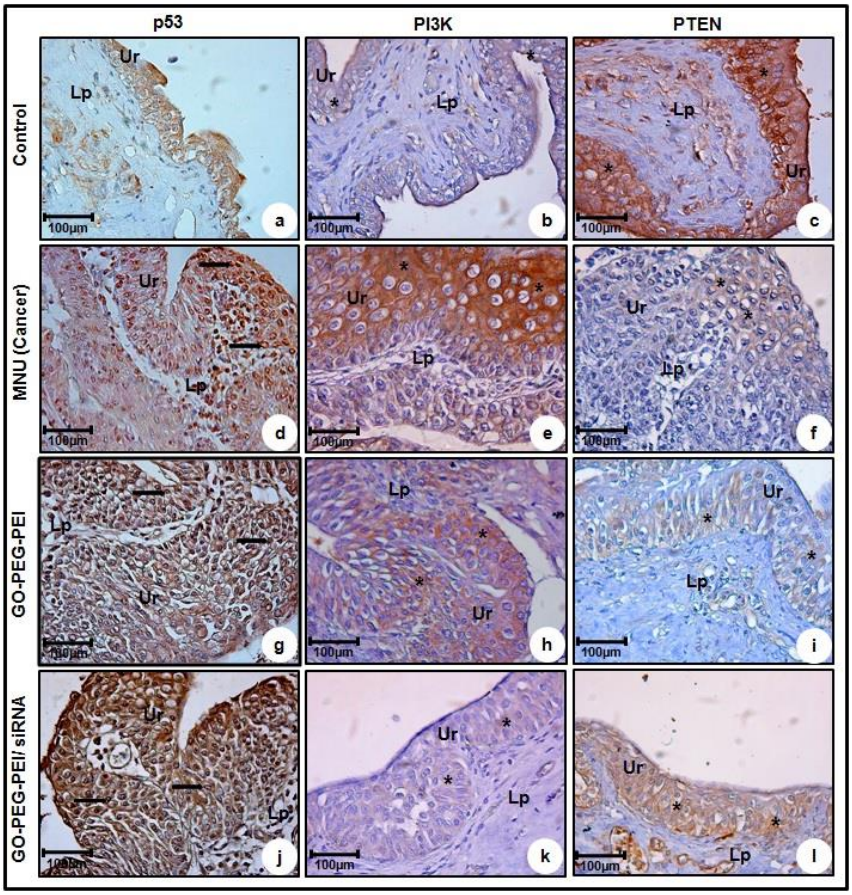

Figure S1. Immunolabelled antigen intensities of the urinary bladder from the Control (a, b), MNU (c, d), GO-PEG-PEI (e, f) and GO-PEG-PEI/ siRNA (g, h) groups. (a), (d), (g) and (j): Immunostaining for p53 (Arrows) in the urothelium. (b), (e), (h) and (k): Immunostaining for PI3K (*) in the urothelium. (c), (f), (i) and (l): Immunostaining for PTEN (*) in the urothelium. Lp: lamina propria, Ur: urothelium.

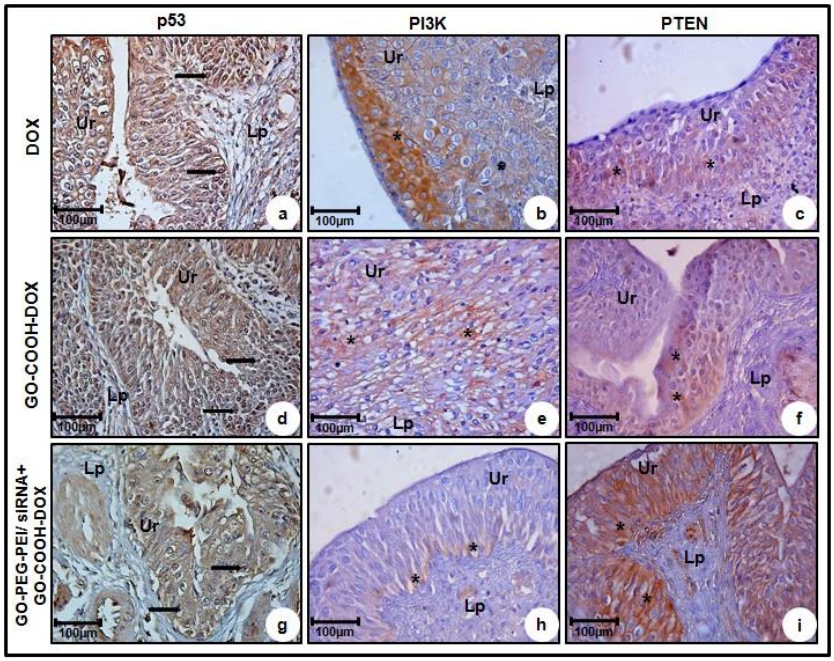

Figure S2. Immunolabelled antigen intensities of the urinary bladder from the DOX (a, b), GO-COOH-DOX (c, d) and GO-COOH-DOX + GO-PEG-PEI/siRNA (e, f) groups. (a), (d) and (g): Immunostaining for p53 (Arrows) in the urothelium. (b), (e) and (h): Immunostaining for PI3K (*) in the urothelium. (c), (f) and (i): Immunostaining for PTEN (*) in the urothelium**. Lp**: lamina propria; **Ur:** urothelium.

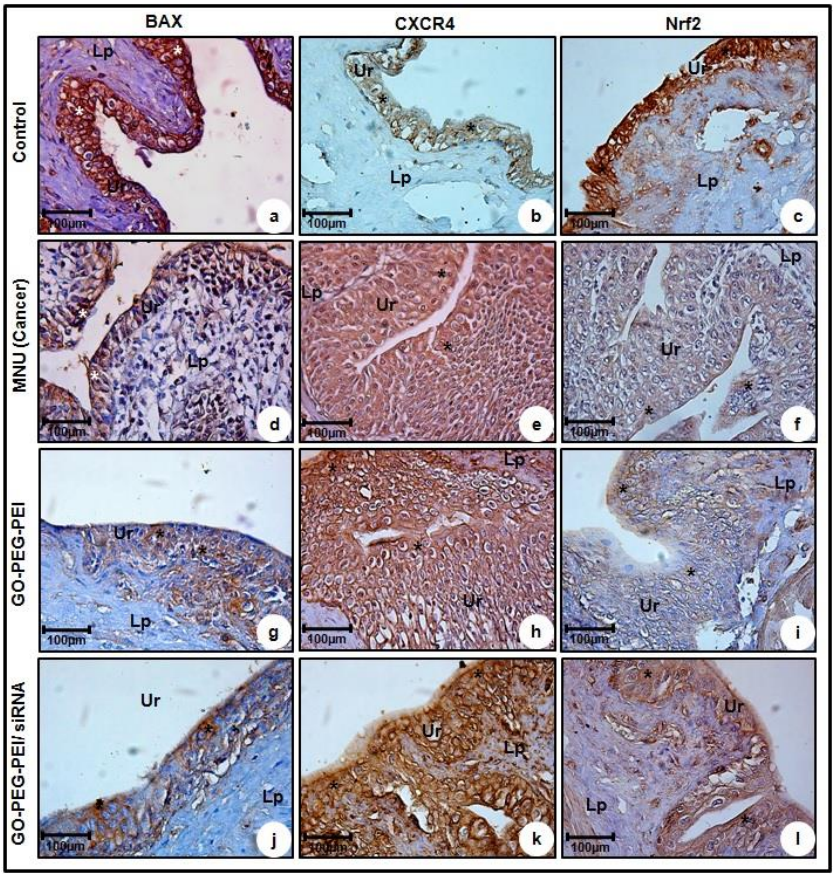

Figure S3. Immunolabelled antigen intensities of the urinary bladder from the Control (a, b), MNU (c, d), GO-PEG-PEI (e, f) and GO-PEG-PEI/siRNA (g, h) groups. (a), (d), (g) and (j): Immunostaining for BAX (*) in the urothelium. (b), (e), (h) and (k): Immunostaining for CXCR4 (*) in the urothelium. (c), (f), (i) and (l): Immunostaining for Nrf2 (*) in the urothelium. Lp – lamina propria, Ur – urothelium.

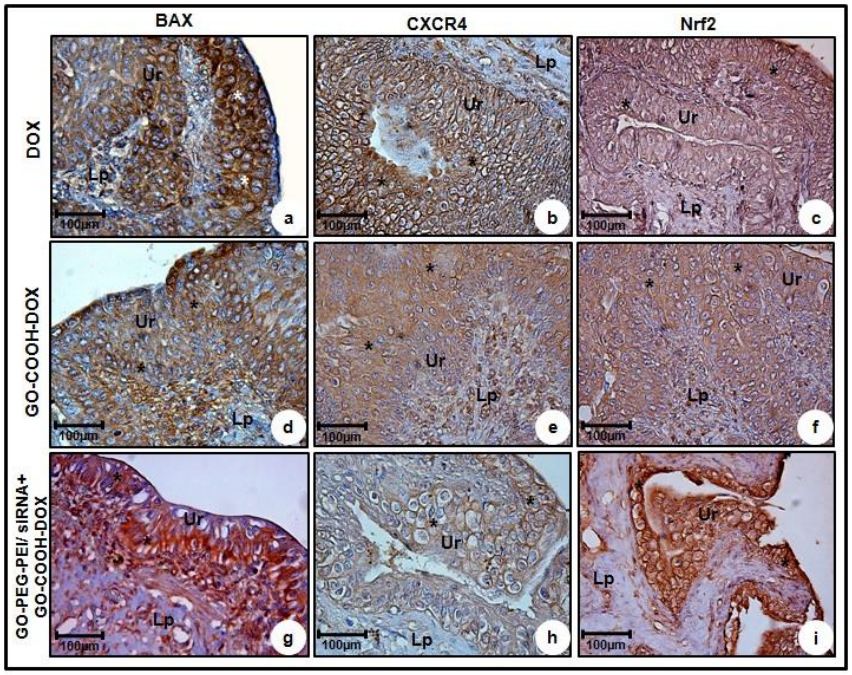

Figure S4. Immunolabelled antigen intensities of the urinary bladder from the DOX (a, b), GO-COOH-DOX (c, d) and GO-COOH-DOX + GO-PEG-PEI/siRNA (e, f) groups. (a), (d) and (g): Immunostaining for BAX (*) in the urothelium. (b), (e) and (h): Immunostaining for CXCR4 (*) in the urothelium. (c), (f) and (i): Immunostaining for Nrf2 (*) in the urothelium. Lp: lamina propria, Ur: urothelium.